Mapping of Near-Surface Winds in Hurricane Rita Using Finescale Radar, Anemometer, and Land-Use Data

KAREN KOSIBA AND JOSHUA WURMAN

Center for Severe Weather Research, Boulder, Colorado

FORREST J. MASTERS

University of Florida, Gainesville, Florida

PAUL ROBINSON

Center for Severe Weather Research, Boulder, Colorado

(Manuscript received 14 December 2012, in final form 29 April 2013)

ABSTRACT

Data collected from a Doppler on Wheels (DOW) mobile radar deployed in Port Arthur, Texas, near the point of landfall of Hurricane Rita (2005) and from two Florida Coastal Monitoring Program 10-m weather stations (FCMP-WSs) are used to characterize wind field variability, including hurricane boundary layer (HBL) streaks/rolls, during the hurricane's passage. DOW data, validated against nearby weather station data, are combined with surface roughness fields derived from land-use mapping to produce fine spatial scale, two-dimensional maps of the 10 m above ground level (AGL) open-terrain exposure and exposure-influenced winds over Port Arthur. The DOW collected ~3000 low-elevation radar sweeps at 12-s intervals for >10 h during the passage of the hurricane. This study focuses on the 2–3-h period when the western eyewall passed over Port Arthur. Finescale HBL wind streaks are observed to have length scales of O(300 m), smaller than previously identified in other HBL studies. The HBL streaks are tracked as they pass over an FCMP-WS located in flat, open terrain and another FCMP-WS located near a subdivision. DOW data collected over the FCMP-WS are reduced to anemometer height, using roughness lengths calculated from DOW and FCMP-WS data. Variations in the radar-observed winds directly over the FCMP-WS are very well correlated, both in their timing and magnitude, with wind gusts observed by the weather stations, revealing directly for the first time the surface manifestation of these wind streaks that are observed frequently by radar >100 m AGL. This allows for the generation of spatially filled maps of small-scale wind fluctuations over Port Arthur during the hurricane eyewall's passage using DOW-measured winds.

1. Introduction

Due to the extreme temporal and horizontal spatial variability of the winds in the hurricane boundary layer (HBL), finescale observations over a broad area are needed to accurately represent the HBL wind structure. Targeted surface observations of HBL winds near the point of landfall with anemometer arrays have occurred in recent years (e.g., Schroeder and Smith 2003; Masters et al. 2010), but these measurements still represent sparse (compared to the radar-observed spatial variability; see below) point observations. Therefore, the two-dimensional details of the HBL structure are not well resolved, and peak/extreme wind events are very likely not sampled. This lack of coverage complicates the reconstruction of the surface wind field and, as a result, objective wind analyses employ sparse data to derive near-surface wind maps over hurricane-impacted areas (Powell and Houston 1996; Powell et al. 1996). Errors in wind field mapping result in spatially aliased characterizations of winds and potentially erroneous predictions/evaluations of structural damage, complicating the diagnosis of the causes of insured and uninsured losses and our understanding of the relationship between intense HBL wind variability and damage.

Of particular interest is the impact of linearly organized coherent wind features in the HBL (e.g., Wurman and Winslow 1998, hereafter W98; Morrison et al. 2005, hereafter M05; Lorsolo et al. 2008, hereafter L08) on the

Corresponding author address: Dr. Karen A. Kosiba, Center for Severe Weather Research, 1945 Vassar Circle, Boulder, CO 80305. E-mail: kakosiba@cswr.org

DOI: 10.1175/MWR-D-12-00350.1

modulation of surface wind speeds. These are thought to be manifestations of "roll" circulations embedded within the HBL with a typical spatial scale of <1 km. It has been hypothesized that the rolls are associated with localized swaths of enhanced wind speeds (W98) and also modify hurricane intensity through the transport of momentum, heat, and water vapor throughout the HBL (e.g., Foster 2005; M05; Kosiba et al. 2012; Kosiba and Wurman 2013, manuscript submitted to *Mon. Wea. Rev.*). Given the small spatial scale, even specialized instrumented weather station arrays (e.g., Schroeder and Smith 2003; Masters et al. 2010), typically spaced at intervals of tens of kilometers, cannot resolve this phenomenon. (It would require hundreds of instrumented weather stations spaced at intervals of $\ll$1 km to resolve explicitly these structures over even a small several square kilometer domain.) Finescale two- and three-dimensional radar observations of the HBL (e.g., W98, L08) have provided much finer-scale spatial coverage of these features, though mainly at heights well above the standard wind measurement height of 10 m above ground level (AGL). In Hurricanes Isabel and Frances, L08 used observations from a mobile radar (beam height of 20–30 m AGL) and a 10-m anemometer to correlate HBL features observed at 20–30 m AGL with surface (10 m AGL) wind data. While L08 did find that the HBL features observed by radar were manifested in the anemometer data, local surface roughness influences have not been identified, and the 20–30 m AGL radar measurements and 10 m AGL anemometer measurements were nearly exactly collocated. Nearly all radar observations are several tens of meters to >100 m AGL (a 1° elevation radar beam is centered over 50 m AGL at ranges >3 km). Whether the frequently observed radar-observed wind streaks/variations >100 m AGL correlate to surface wind fluctuations has not been demonstrated.

To fully incorporate HBL wind variability into meteorological, engineering, and hazard models, it is necessary to augment our current knowledge of internal hurricane dynamics with a complete characterization of these critical flow-modulating processes at scales sufficiently fine to fully resolve their quantitative structure, and understand their intensity, frequency, and evolution throughout the HBL down to the surface.

2. Overview of Hurricane Rita and data collection

The National Hurricane Center (NHC) estimated that Rita made landfall as a Saffir–Simpson hurricane wind scale category 3 hurricane with sustained winds >50 m s^{-1} (100 kt) at 0740 UTC on 24 September, just west of Johnson's Bayou, Louisiana, and just east of Sabine Pass, Texas, near the Texas–Louisiana border. The strongest sustained wind (2-min average) measured at an official recording station (SRST2[1]), in Sea Rim State Park, Texas, was 36.5 m s^{-1} (71 kt) with peak gusts of 44 m s^{-1} (86 kt) at 0700 UTC (Beven et al. 2008) (Fig. 1).

A Doppler on Wheels mobile radar (DOW; Wurman et al. 1997; Wurman 2001), deployed at the south edge of Port Arthur, Texas (29.88402°N, 93.98774°W), began data collection at 2148 UTC on 23 September, approximately 10 h prior to landfall. DOW data collection ended at 1253 UTC on 24 September. The DOW was located on a highway overpass at an elevation of approximately 10 m AGL, where the local ground elevation was approximately 1–2 m above mean sea level (MSL). This site was chosen to provide safety from the forecast storm surge, while being approximately downwind of two instrumented weather stations (T0 and T3) described below (Figs. 2 and 3). The DOW heading was 138.2° ± 0.1°, as determined by a solar alignment, and level to within 0.2°.

The DOW transmitted 0.167-μs pulses and sampled at 0.167-μs intervals, resulting in nonoversampled 25-m gate lengths. The 2.44-m antenna produced a 0.93° beamwidth and data were azimuthally oversampled to 0.3°, producing samples every 26 m at a range of 5.0 km, and approximately 45 m at the range of the weather stations (see below). For nearly the entire deployment, the DOW scanned out to a range of 9.37 km in a rapid-scanning mode at one elevation (1.2°),[2] collecting an unprecedented 3000 two-dimensional low-level data samples every 11–12 s, in order to optimize two-dimensional observations of HBL streaks/rolls.

The Florida Coastal Monitoring Program (Balderrama et al. 2011) deployed the T0 and T3 weather stations in the Port Arthur area. T0 was deployed at the Jack Brooks Regional Airport, which serves the Beaumont–Port Arthur area (BPT; 29.9512°N, 94.0220°W), and T3 was deployed in a field in the nearby town of Nederland, Texas (29.9548°N, 93.9542°W) (Figs. 2 and 3). The elevation of the ground at both of these sites was approximately 5 m MSL. Each weather station had an anemometer at 10 m AGL, which recorded data at 10 Hz. Relative to the DOW, T0 was located 336.2° at a distance of 8.15 km, and T3 was 22.3° at a distance of 8.49 km (Fig. 1). At these ranges, DOW data were collected at altitudes (radar beam centers) of 171 ± 27 m and 178 ± 27 m above the heights of the anemometers mounted on T0 and T3, respectively (the half-power beamwidth was ~120 m at this range). This analysis focuses on characterizing the HBL rolls and

[1] The measurement was taken at approximately 9.8 m MSL over marshland.

[2] Refineries north of the DOW deployment site contained structures that blocked the radar beams below 0.5°–1.0° in a majority of the sectors. A few small sectors were obstructed even at 1.2° elevation and data from these sectors were removed from the analysis.

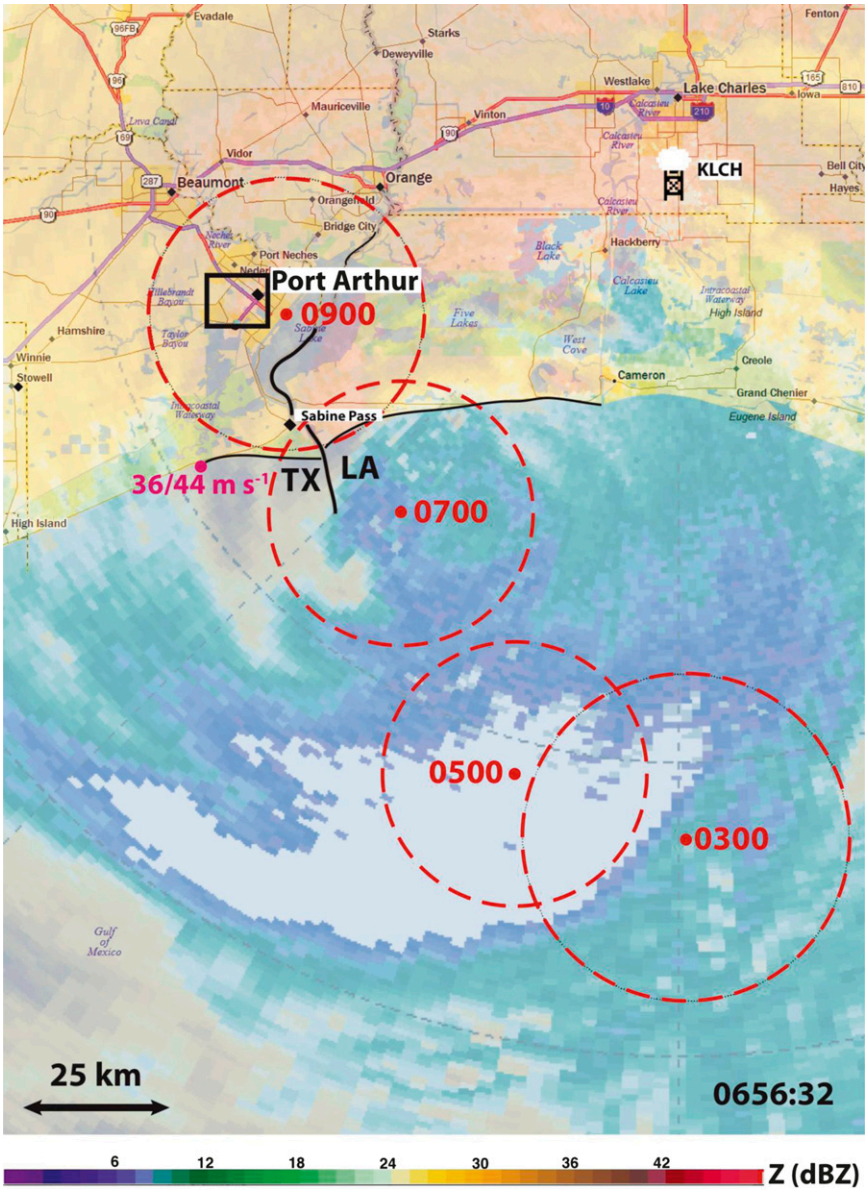

FIG. 1. Overview of Hurricane Rita's landfall. Shown are Hurricane Rita's reflectivity Z at 0656 UTC, as observed by the Lake Charles, LA, Weather Surveillance Radar-1988 Doppler (WSR-88D); the center and approximate diameter of the inner eyewall of Hurricane Rita at 0300, 0500, 0700, and 0900 UTC (red annotations); the location of the highest wind speed observation, as recorded by an official observing station (magenta dot); and the approximate location of the analysis domain, which is shown in greater detail in Fig. 2 (black rectangle).

mapping the near-surface HBL winds between 0600 and 0900 UTC, as Hurricane Rita made landfall and the strongest winds impacted Port Arthur.

3. Hurricane boundary layer roll characteristics

Hurricane boundary layer wind streaks/rolls, characterized by a spatial periodicity in wind speed (e.g., W98, L08), were present throughout the duration of the passage of Hurricane Rita (Fig. 4). To facilitate analysis of these features, the DOW data were objectively analyzed[3] onto a Cartesian grid using a horizontal grid spacing of $\delta_x = \delta_y = 25$ m. The characteristic wavelength of the streaks/rolls then was determined by calculating

[3] A two-pass Barnes (Barnes 1964) objective analysis scheme (Majcen et al. 2008) was used with $\kappa = 0.0011\ \text{km}^2$ and $\gamma = 0.3$.

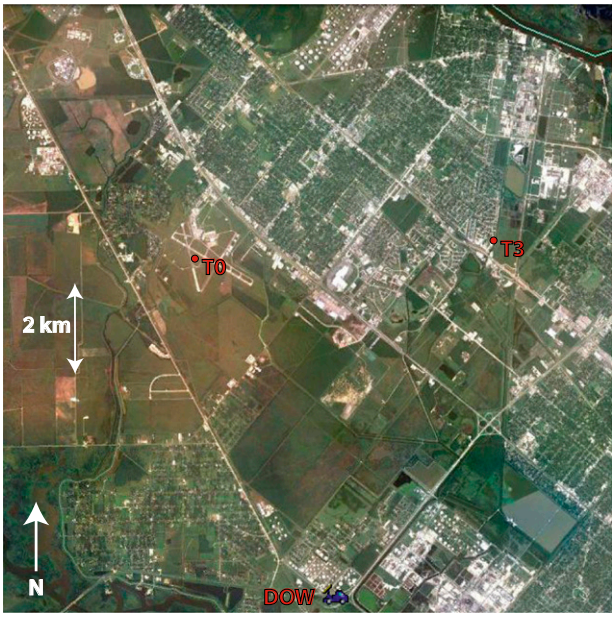

FIG. 2. Zoomed-in aerial imagery of DOW and the meteorological tower (T0 and T3) deployment in Port Arthur. Displayed area corresponds approximately to the black rectangle in Fig. 1.

fast Fourier transforms (FFTs) perpendicular to the long (translational) axis of the streaks/rolls at a range of 5 km from the radar (Fig. 5). At 5-km range, the radar beamwidth is approximately 80 m, so features smaller than ~160 m are not well resolved, but features ~480 m have approximately six samples across them, resolving ~75% of their magnitude (Carbone et al. 1985). To evaluate the effects of radar resolution on this calculation, and the aliasing of wavelengths to false, larger scales, FFTs also were calculated at a range of 2 km from the radar, at which distance features of wavelength ~192 m were substantially resolved (75% of their magnitude).

An FFT analysis was conducted for each radar scan, resulting in approximately 300 FFTs per each hour of analysis. Figure 6 depicts the bin-weighted occurrence of the three highest energy wavelengths for each hour between 0600 and 0900 UTC at ranges of 5 and 2 km from the radar. At both ranges, wavelengths of up to 1.5 km and smaller than 200 m were observed, but the mean wavelengths μ were $O(400\,\text{m})$ and $O(300\,\text{m})$ at ranges of 5 and 2 km from the radar (approximately 47–110 m AGL), respectively. While the values of $O(400\,\text{m})$ are similar to those observed by W98 and L08, the prevalence of the smaller wavelength [$\leq O(300\,\text{m})$] features observed at a range of 2 km from the radar suggests that these were likely underresolved in these previous analyses of the HBL (consistent with Kosiba and Wurman 2013, manuscript submitted to *Mon. Wea. Rev.*) and,

FIG. 3. DOW and tower instruments and Hurricane Rita deployment sites.

thus, aliased to larger scales.[4] The characteristic residual velocities associated with the rolls/streaks at 2- and 5-km range from the radar were determined by subtracting the

[4] Data were not taken at multiple elevations, so the height dependency of the characteristic size cannot be assessed. Although an increase in characteristic size with height cannot be ruled out, the change in radar beam height from 2- to 5-km range was only 60 m, implying that the observed increase in scale was not due to beam height variation.

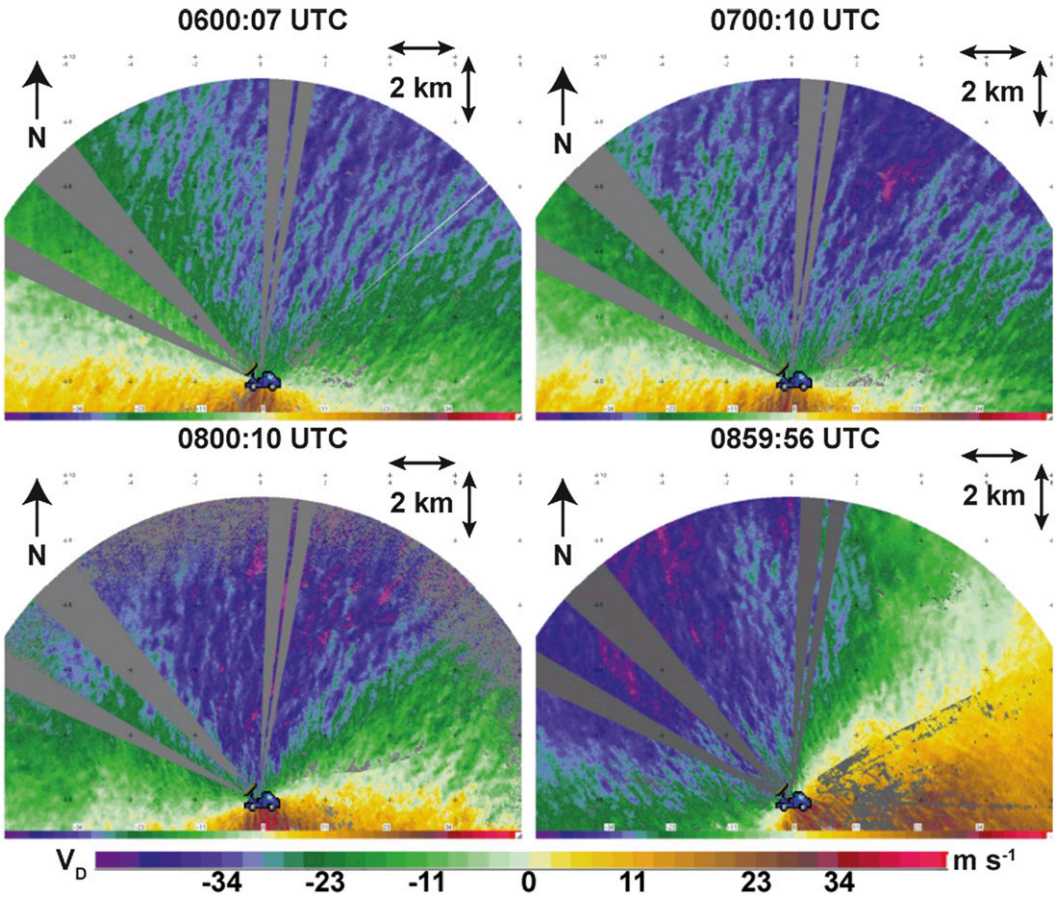

FIG. 4. Doppler velocities V_D from plan position indicator (PPI) scans at 1-h intervals during the study period. The location of the DOW radar is indicated. Boundary layer streaks and other variability are visible as the background wind direction backs from north-northeastward to northwestward during the period. Data from blocked sectors have been removed (gray fill), north is up, and Doppler velocities are contoured from $\pm 47.25\,\mathrm{m\,s^{-1}}$ in $2.25\,\mathrm{m\,s^{-1}}$ increments.

average winds, derived from velocity azimuthal display analyses at each time, from the Doppler velocities. For wavelengths between 200 and 800 m, the perturbation velocities were typically 4–6 $\mathrm{m\,s^{-1}}$, although some values exceeded $10\,\mathrm{m\,s^{-1}}$, particularly at distances close (2 km) to the radar. The residual velocities are comparable to the values observed by L08 (typically ranging from $\pm 6\,\mathrm{m\,s^{-1}}$), although L08's analyses did not reveal any residual velocities exceeding $10\,\mathrm{m\,s^{-1}}$. W98 qualitatively identified residual velocities approaching $13\,\mathrm{m\,s^{-1}}$, but these values likely were associated with only the most prominent features. Kosiba and Wurman (2013, manuscript submitted to *Mon. Wea. Rev.*) found smaller average residual velocities in a finescale dual-Doppler analyses of the HBL of Hurricane Frances.

4. Time history of winds and surface roughness

To study the relationship between radar-measured Doppler winds at ~175 m AGL with anemometer-measured winds at 10 m AGL, the anemometer wind speeds have been normalized by the radar-viewing angle using the following relation:

$$V_t = V_0 \times \cos(\theta - \Delta\theta),$$

where V_0 is the weather-station-measured wind speed, θ is the weather-station-observed wind direction, $\Delta\theta$ is the angular offset from north of the anemometer location to the DOW, and V_t is the component of V_0 in the direction of the DOW beams. The Doppler wind speeds measured by the DOW at the weather stations' locations were determined by taking the average Doppler velocity V_D measurement within a nominal horizontal distance ("patch") from the weather station location. For this study, we used a 50-m radius patch,[5] which, assuming

[5] A 50-m patch represents an average of the radar data within a 50-m radius of a given location.

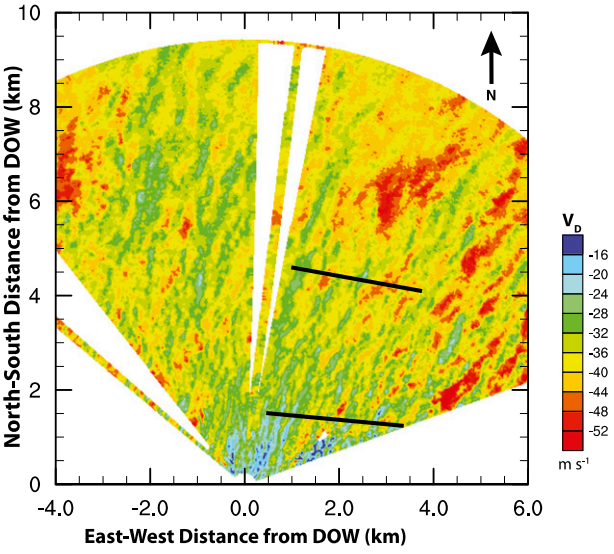

FIG. 5. An example of objectively analyzed Doppler velocity V_D to a horizontal plane (z = 100 m AGL) at 0710:10 UTC. The objective analysis captures much of the subkilometer-scale variability, particularly close to the radar. The 2- and 5-km-range cross-sectional locations used in the FFT analysis (shown in Fig. 6) are depicted as black line segments.

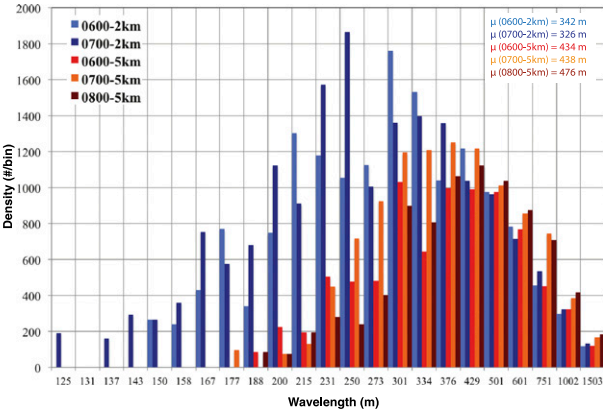

FIG. 6. FFT analysis at 2- and 5-km range from the DOW during three 1-h periods starting at the indicated times. The value of mean wavelengths for each time and location are given in the top-right corner of the plot. Insufficient data were available at 5-km range from 0800 to 0900 UTC.

a representative wind speed of ~30 m s^{-1}, corresponds approximately to a ~3-s gust wind speed that is commonly employed in many building standards (e.g., ASCE 2010).

Figures 7a and 8a depict the normalized wind speeds observed by T0, T3, and the 50-m patch DOW winds observed at the weather stations' locations from 0600 to 0900 UTC. The magnitude of these winds increased through approximately 0840 UTC, and then decreased after as the eyewall moved northward and out of the observation domain. Correspondingly, through 0800 UTC, the wind direction (not shown) was predominantly northerly (varying approximately ±15°), progressively becoming northwesterly after 0800 UTC. Doppler velocities measured by the DOW are stronger than those measured by the weather stations primarily owing to the height difference between the DOW radar samples and the weather station anemometers. Following a similar approach to Franklin et al. (2003) and Kepert (2006), in order to remove the height dependence from the radar observations, wind reduction factors (RFs) of 0.73 and 0.45 were chosen based on minimization of the root-mean-square difference between the weather station and DOW mean winds from 0700 to 0800 UTC[6] and then were applied to the DOW data to match the T0 and T3 observations. Since the DOW observations were at approximately the same height above T0 and T3, the disparate RFs are likely indicative of different surface roughness conditions influencing the winds at the T0 and T3 locations.

While a recent study suggests that the winds in the HBL may deviate from a logarithmic profile (Smith and Montgomery 2013), many observations of hurricane winds over the open ocean suggest that winds below the height of the low-level wind maximum can be approximated by a logarithmic profile (e.g., Powell et al. 2003; Franklin et al. 2003; Vickery et al. 2009; Giammanco et al. 2013). However, at surface roughness discontinuities such as the ocean–land interface or changes in surface roughness conditions, one or more internal boundary layers can develop (e.g., Powell et al. 1996; Hirth et al. 2012), complicating the low-level vertical wind profile. As such, the extent to which the upstream surface conditions in heterogeneous terrain influence the wind measurements at a particular point is not known (Hirth et al. 2012). Given these constraints, a simple logarithmic wind profile was used in this study to approximate the surface roughness values at the locations of T0 and T3. Using the RFs derived earlier, and assuming a neutrally stable boundary layer,[7] the roughness lengths characteristic of the T0 and T3 locations were calculated using the following relationship:

[6] The 0800 to 0900 UTC interval was excluded because the wind direction varied appreciably during this period.

[7] The assumption of a neutrally stable boundary layer is based on the nocturnal hurricane environment; specifically, the boundary layer should be well mixed due to the overturning associated with the rolls/streaks and there should be little net surface heating–cooling due to cloud cover.

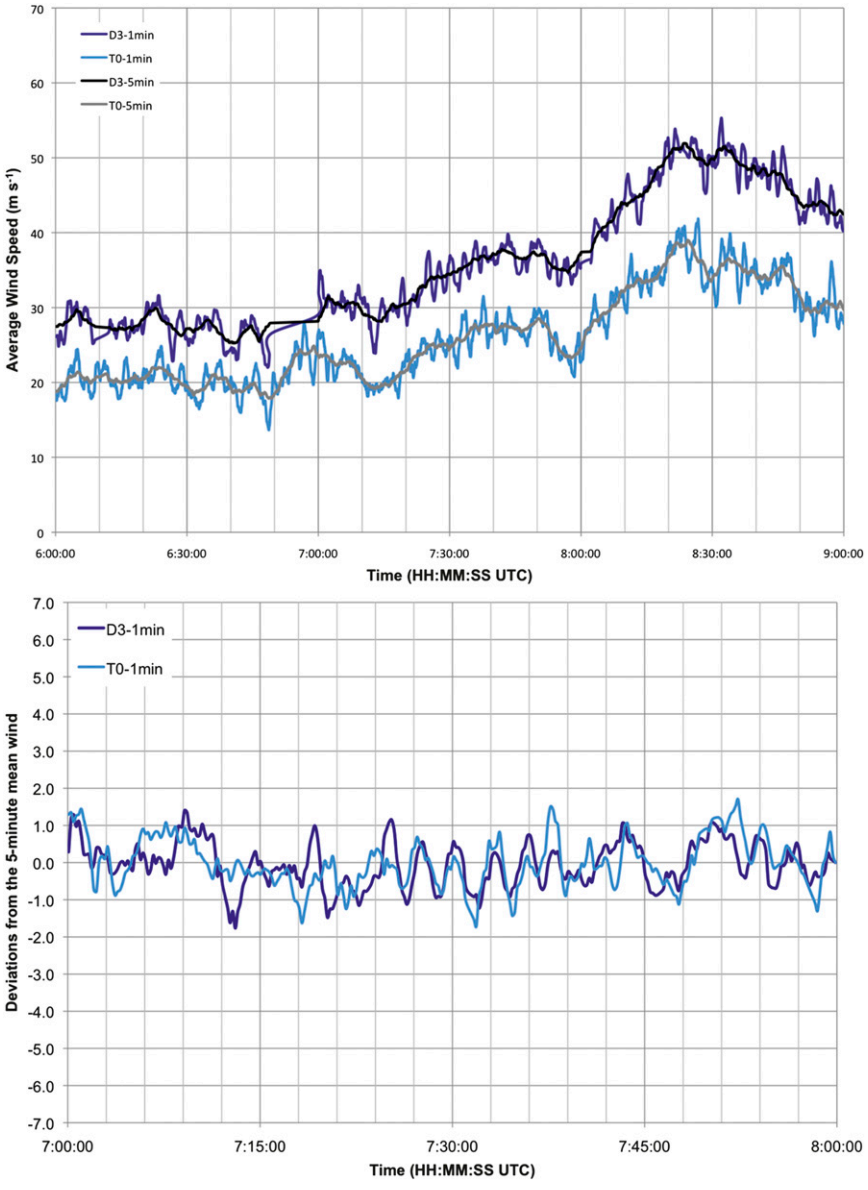

FIG. 7. (top) Time series of the 1-min-average (colored lines) and 5-min-average (grayscale lines) winds from 0600 to 0900 UTC observed by T0 and by the DOW at the location of T0. (bottom) Deviation of the 1-min-average winds from the 5-min-average wind for T0 and the DOW winds observed at T0 from 0700 to 0800 UTC. Tower winds have been normalized by radar-viewing angle and the DOW winds are constructed from a 50-m patch. Both tower and DOW winds have been averaged in 1-min overlapping blocks.

$$z_0 = \exp\left[\frac{\ln(h_t - z_d) - \dfrac{V_t}{V_D}\ln(z - z_d)}{1 - \dfrac{V_t}{V_D}}\right],$$

where h_t is the height of the weather station (10 m AGL), z is the height of the DOW wind observation (m AGL) at the weather station location, z_d is the zero-plane displacement height, and z_0 is the roughness length. The RF of 0.73 that was applied to the DOW data at T0 and corresponded to a calculated roughness length of 0.004 m. Since T3 is located at a boundary between a relatively densely built-up subdivision and an open field (Fig. 2), it was necessary to use a nonzero displacement height z_d after 0700 UTC, when the wind direction changed to a north-northeasterly direction that was parallel to the boundary between the two different terrain types. Using a 0.45 RF that was applied

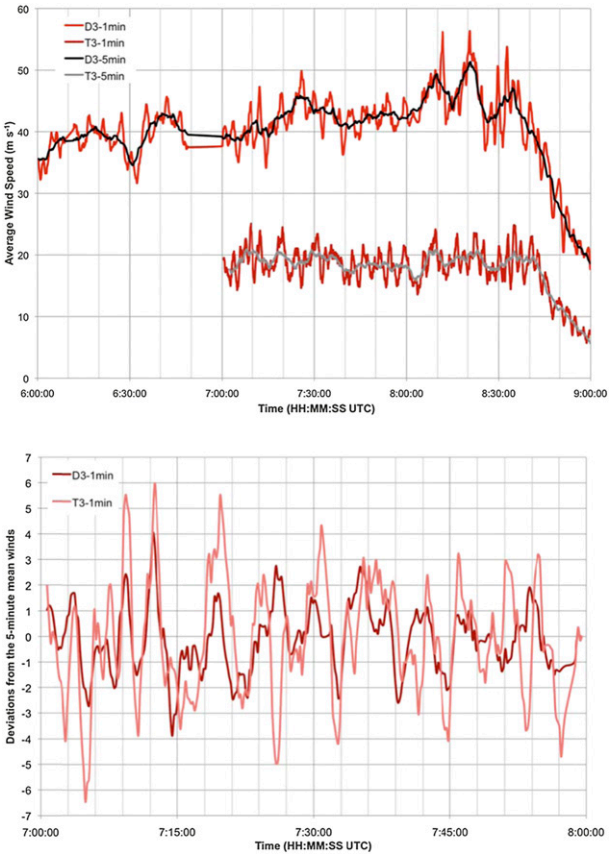

FIG. 8. (top) Time series of the 1-min-average (colored lines) and 5-min-average (grayscale lines) winds from 0600 to 0900 UTC observed by T3 and by the DOW at the location of T3. (bottom) Deviation of the 1-min-average winds from the 5-min-average wind for T3 and the DOW winds observed at T3 from 0700 to 0800 UTC. Tower winds have been normalized by radar-viewing angle and the DOW winds are constructed from a 50-m patch. Both tower and DOW winds have been averaged in 1-min overlapping blocks.

to the DOW data at the T3 location and a displacement height of 4 m, based on the recommendation of Wieringa (1993), a roughness length of 0.36 m was calculated at the T3 location. The roughness length at T0 fit within the range of characteristic values of mown grass [0.001–0.01 m; Simiu and Scanlan (1996)] and z_0 for T3 was close to the range of characteristic values for a suburb [0.4–0.7 m; Wieringa (1993)]. These values and corresponding descriptions also are reasonably representative of the land surface types at the weather station locations, as determined from satellite and ground-based images, at the weather stations' locations (Fig. 2).

To focus on the small-scale wind speed trends associated with the observed coherent wind field structures, the 5-min running mean $\mu_{5\text{min}}$ was subtracted from the 1-min mean wind speed $V_{1\text{min}}$ and then normalized by the standard deviation $\sigma_{1\text{hr}}$ for the DOW and for the weather station observations between 0700 and 0800 UTC (Figs. 7b and 8b):

$$\frac{V_{1\text{min}} - \mu_{5\text{min}}}{\sigma_{1\text{hr}}}.$$

The correlations between the 1-min mean wind speeds observed by the weather stations (T0 and T3) and by the DOW were determined by calculating the correlation coefficients for these quantities during this 1-h period. For the 1-min mean wind speed, the correlation coefficients between the DOW and weather station wind deviations from the 5-min mean were +0.52 for T0 and +0.47 for T3, indicating a statistically significant relationship (at the $\alpha = 0.05$ level) between the radar and the anemometer observations. The correlation coefficients for 3-s gusts were +0.35 for T0–DOW and +0.21 for T3–DOW.

Using the method described in the appendix, the DOW observations from above the locations of T0 and T3 were adjusted down to the anemometer heights of 10 m AGL from 0400 to 1000 UTC and from 0700 to 0800 UTC, respectively (Figs. 9 and 10). Figures 9b and 9c depict the 10-min-average wind speed and longitudinal turbulence intensity, respectively, for T0 and the DOW observations at the T0 location. Once the DOW observations were adjusted to the anemometer height, both the wind speed and turbulence intensity generally correlated well between the DOW and weather station measurements. The expected wind speed values fall within the upper and lower bound confidence levels of 0.95 and 0.05, respectively, at all but a few times, indicating that the 10-min wind variations observed aloft are representative of the surface winds. A similar analysis was conducted for the T3 measurements and corresponding DOW observations between 0700 and 0830 UTC with $z_d = 4$ m, yielding good agreement between the adjusted-DOW measurements and the T3 measurements (Fig. 10).

The agreement between the 1- and 10-min variabilities in the DOW and the anemometer wind data, when corrected for observation height, geometry, and derived exposure, confirm that the subkilometer wind streaks, as revealed by velocity perturbations in the DOW data >100 m AGL, are closely correlated with surface wind fluctuations. Consequently, these subkilometer features observed by the DOW at ~180 m AGL are coherent down to the 10 m AGL level, particularly in open and/or homogeneous exposure areas (e.g., T0).

5. Two-dimensional wind maps

The demonstrated correlation between the DOW-measured winds and the anemometer point measurements motivates the creation of highly detailed two-dimensional area-wide surface wind maps over Port

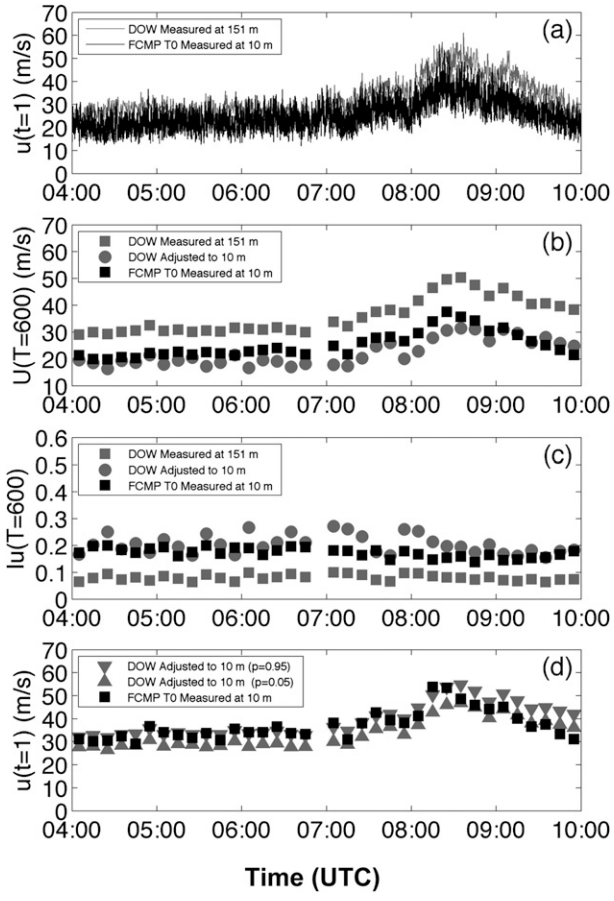

FIG. 9. The (a) 1-s wind observations from T0 and the DOW at the T0 location; (b) 10-min average winds for T0, DOW at the T0 location, and 10-m adjusted DOW; (c) turbulence intensity for T0, DOW at the T0 location, and 10-m adjusted DOW; and (d) the expected 10-m adjusted DOW winds and T0 winds for derived z_0.

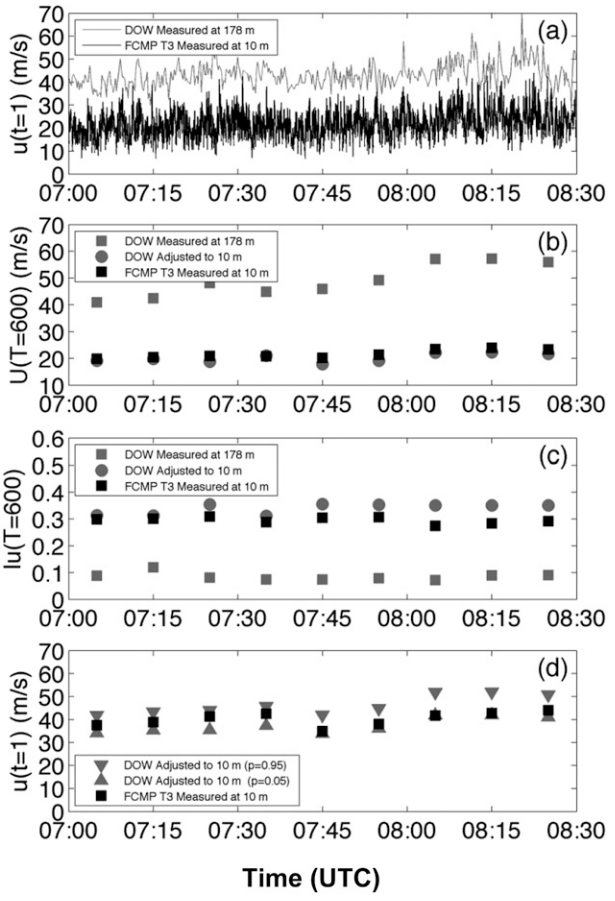

FIG. 10. The (a) 1-s wind observations from T3 and the DOW at the T3 location; (b) 10-min average winds for T3, DOW at the T3 location, and 10-m adjusted DOW; (c) turbulence intensity for T3, DOW at the T3 location, and 10-m adjusted DOW; and (d) expected 10-m adjusted DOW winds and T3 winds for derived z_0.

Arthur using the space-filled DOW wind data. Corresponding to the DOW data coverage over Port Arthur, a 10 km × 10 km mapping domain was chosen and partitioned into 1600 squares of 0.25 km × 0.25 km in order to account for the effects of the inhomogeneous surface roughness on the 10-m radar-derived winds. Each of the 1600 squares was assigned a roughness length z_0 based on land use within that segment. Land use was determined through the use of Google Earth images, the National Oceanic and Atmospheric Administration Coastal Change Analysis Program (C-CAP) land-use data, and corresponding z_0 values obtained from the Federal Emergency Management Agency's multihazard Methodology for Estimating Potential Losses from Disasters (HAZUS-MH; FEMA 2006), which provides ranges of surface roughness length values from several sources. Roughness lengths varied from ~1.0 over densely built-up areas to 0.01 over water surfaces and wetlands (Fig. 11). The DOW velocities were objectively analyzed onto a Cartesian grid with a horizontal grid spacing of 25 m (see footnote 2) and then reduced to 10 m AGL using the logarithmic profile described above, in accordance with the assigned roughness length values.[8] To minimize errors in wind speed due to the radar observation angle relative to the true wind direction, only DOW data in a sector extending ±30° from the mean wind direction were used to generate the wind map. [DOW data within this sector were still normalized using wind direction, but these corrections did not exceed 1/cos(30°) = 1/0.87.]

Maximum 1-min-average winds at 10 m AGL for the 0600–0900 UTC period were derived from the DOW

[8] As discussed earlier, while the upstream fetch does influence the wind speed at a particular location, due to the complex terrain and the likely development of multiple internal boundary layers, the distance of the upstream influence is unknown so the local surface roughness values were used to construct these maps.

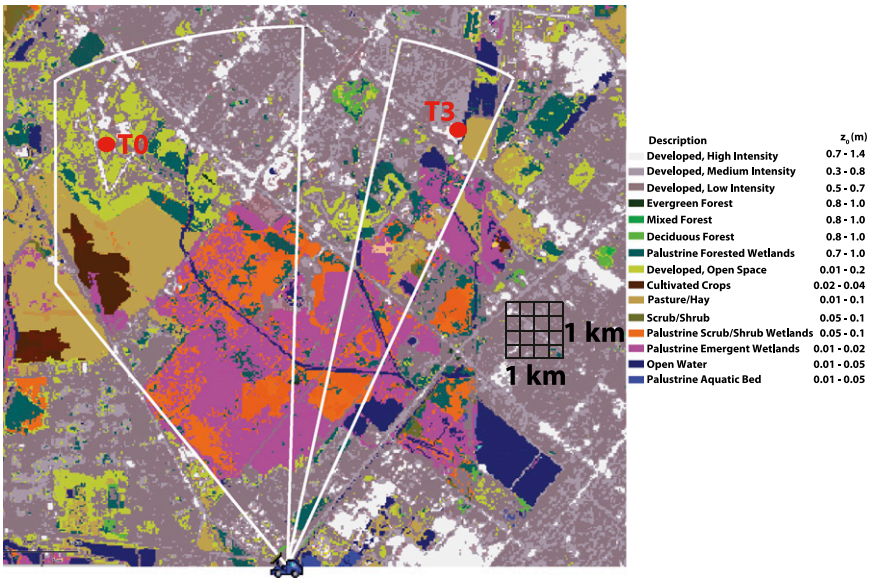

FIG. 11. C-CAP land-use map over Port Arthur (http://www.csc.noaa.gov/ccapatlas/) and the range of surface roughness values used for each type of usage. Example of the 250 m × 250 m surface roughness grid used to convert the DOW winds into 10 m AGL winds is shown. Locations of the DOW and the towers are indicated. The DOW domain over which the two-dimensional wind maps were derived is outlined in white.

velocities using the varied land-usage distribution of Port Arthur (Fig. 12, top) and using a uniform surface roughness value typical of open-exposure terrain (z_0 = 0.03 m) (Fig. 12, bottom). Not only do the derived wind speeds at a particular location vary as a function of surface roughness, but they also exhibit variations due to the presence of the boundary layer streaks and other larger-scale HBL features. The peak wind map using the open-exposure terrain surface roughness over the entire domain preserved the meteorologically caused variation, but overrepresented the magnitude of the surface winds in built-up areas. The DOW-derived and anemometer-measured winds closely agree early in the landfall period. However, the DOW-derived winds overestimate the winds measured at T3 after 0800 UTC. As T3 was at a boundary between relatively open and obstructed exposures, when the winds at T3 backed to a northwesterly direction after 0800 UTC, the upstream fetch was over the more built-up area, reducing the measured wind speeds. Future analysis efforts will incorporate more sophisticated roughness models, including the effects of varying wind directions on the assumed upstream exposure.

The continuous two-dimensional wind speed maps derived using DOW data and surface roughness/exposure adjustments permit estimation of peak wind gusts at locations not sampled by towers. These maps reveal intense peak wind gusts east and south of T3 (arrows in Fig. 12), largely due to more open exposures close to the track of the center of the hurricane, and across two separate regions between the DOW and T0 (ovals A and B in Fig. 12), associated with intense wind streaks passing over open-exposure terrain. Relatively intense wind gusts are evident in a narrow north–south-oriented band approximately 3.8–5.8 km north of the DOW (oval C in Fig. 12), associated with a particularly intense wind streak that passed between (and was thus unmeasured by) the T0 and T3 towers.

6. Conclusions

The HBL of Hurricane Rita comprises quasi-linearly organized coherent structures, which were shown to be well correlated with surface wind fluctuations. Identifying the characteristic size of these subkilometer-scale structures using radar data can be problematic due to the decreasing spatial resolution of the data with increasing range from the radar. The ability to resolve features with sizes ≤200 m close to the radar suggests that these small scales were present throughout most of the radar-observed domain and not well resolved farther from the radar. During the 3-h period including the passage of the eyewall of Rita across Port Arthur and the resultant most intense winds, DOW data revealed little change in the characteristic spatial scale of these structures. While features with a characteristic size of 400 m

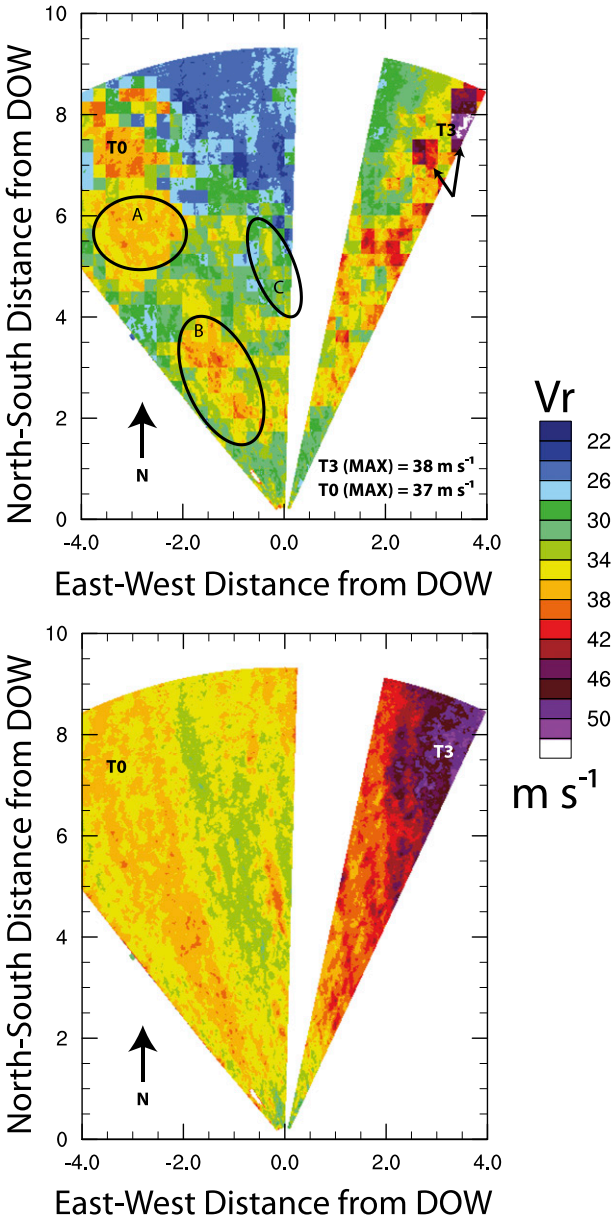

FIG. 12. Maps of 3-h-maximum 1-min-average 10 m AGL surface winds V_r calculated by reducing DOW patch winds to 10 m AGL using surface roughness derived (top) from land use and (bottom) using open-exposure surface roughness (z_0 = 0.03 m). Wind speed is contoured from 22 to 50 m s^{-1} in 2 m s^{-1} increments. T0 and T3 denote the locations of the two towers. Peak DOW-derived winds at T0 and T3 are 37 and 38 m s^{-1}, respectively. Arrows and ovals denote regions of enhanced winds speeds.

are consistent with the observations of W98 and L08, the presence and prevalence of the smaller-scale features (100–200 m) in these observations in Hurricane Rita indicate that earlier studies may have overestimated the true characteristic size of the subkilometer HBL wind streaks/rolls. This has important implications for parameterizations used to calculate fluxes in numerical models of hurricanes.

Comparisons between DOW wind observations >100 m AGL and wind gust measurements obtained by 10 m AGL instrumented weather stations below the DOW observation level revealed close agreement after adjustments for surface roughness and geometry. DOW-observed wind streaks at ~175 m AGL are well correlated with 1-min surface wind fluctuations and less, but still positively, correlated with 3-s wind fluctuations. Radars have measured wind streaks at >100 m AGL in several landfalling hurricanes, but this is the first time that these >100 m AGL features have been associated directly with 10 m AGL anemometer-measured wind fluctuations. When the DOW wind observations were corrected for observation geometry and height, short-time-scale winds were well correlated with the anemometer observations, with correlation coefficient values of 0.52 and 0.47 for T0 and T3, respectively. Surface roughness values were derived from the DOW- and weather station-observed winds and these values agreed reasonably well with the expected roughness values of the underlying surfaces. Turbulence intensity statistics were used to reduce DOW-observed winds to tower height, yielding good agreement between DOW and tower observations.

Motivated by the close correlation between the DOW-measured winds and the anemometer-measured surface wind fluctuations using two different methodologies, the DOW data were employed to construct spatially continuous two-dimensional maps of peak surface winds in the varying surface roughness conditions of Port Arthur, Texas. Maps of average winds and 1-min peak winds over individual neighborhoods, industrial assets such as refineries, and open-water areas reveal spatial and temporal variations in near-surface wind speeds due to both meteorological and exposure/roughness variations. In particular, variations due to meteorological fluctuations (the most intense portions of wind streaks) passing between surface anemometers are revealed and mapped. This technique can be used in other landfalling hurricanes to identify where peak winds may be associated with localized areas of enhanced damage.

Acknowledgments. NSF Grant AGS-0910737 supported this work. The DOWs are NSF Lower Atmospheric Observing Facilities supported by Grant AGS-0801041. The authors thank Rita crewmembers for the collection of the DOW and tower data, Curtis Alexander for his DREADER analysis package, Rachel Humphrey for her

assistance in preparing the manuscript, and the reviewers for their helpful input.

APPENDIX

Calculation of the Turbulence Intensity Statistics

The longitudinal turbulence intensity I_{ur} was calculated as follows:

$$I_{\mathrm{ur}} = \frac{\sigma_{\mathrm{ur}}}{U_r}, \tag{A1}$$

where the mean horizontal velocity U_r is calculated from V_t for T-duration (e.g., 10 min) nonoverlapping intervals and the standard deviation of the along-wind component σ_{ur} is calculated from

$$\sigma_{\mathrm{ur}} = \frac{\sigma_{\mathrm{ur,measured}}}{\int_0^{\infty} S(n, z, z_0)\chi^2(n)\, df}, \tag{A2}$$

where $\chi^2(n)$ is the low-pass, block-averaged filter as described in Beljaars (1987):

$$\chi^2(n) = \left[\frac{\sin(n\pi t)}{n\pi t}\right]^2 \frac{1}{N^2}\left[\frac{\sin(\pi n\Delta N)}{\sin(\pi n\Delta)}\right]^2, \tag{A3}$$

where n is the sampling frequency (in Hz), $S(n, z, z_0)$ is the one-sided power spectral density of the longitudinal turbulence, t is the duration of the nonoverlapping block average, N is the number of samples in the average, Δ is the time interval between samples, and the integration is performed over frequency (f, in Hz). In this study, the von Kármán form of $S(n, z, z_0)$ was used (Greenway 1979):

$$\frac{f \times S(n)}{\sigma_u^2} = \frac{4n\dfrac{L_u^{\chi}}{U}}{\left[1 + 70.8\left(n\dfrac{L_u^{\chi}}{U}\right)^2\right]^{5/6}}, \tag{A4}$$

where L_u^{χ} is the integral length scale of the wind.

A bounded nonlinear function minimization was performed to find the roughness length z_0 and frictional velocity u_* such that the logarithmic function of the mean wind profile (assuming a neutrally stable boundary layer),

$$U = \frac{u_*}{k}\ln\left(\frac{z}{z_0}\right), \tag{A5}$$

and the modified form of the Harris and Deaves (1981) variance model given in ESDU (1983) and described in Vickery and Skerlj (2005) are satisfied:

$$\sigma = \frac{u_* 7.5n\left[0.538 + 0.09\ln\left(\dfrac{z}{z_0}\right)\right]n^{16}}{1 + 0.156\ln\left(\dfrac{u_*}{fz_0}\right)} \quad \text{and} \tag{A6}$$

$$\eta = 1 - 6f\frac{z}{u_*}, \tag{A7}$$

where $U = U_r$, k is von Kármán's constant (0.41), z is the height of the radar beam, and f is the Coriolis force. Equation (A5) is modified when the displacement height is nonzero (z_d) ($z = z - z_d$).

The equivalent mean wind speed at the surface level U_s is calculated by developing Eq. (A6) for $z = z_s = 10$ m and $z = z_r$ = the height of the radar beam, and setting u_*/k equal to one another:

$$\frac{U_s}{\ln\left(\dfrac{z_s}{z_0}\right)} = \frac{U_r}{\ln\left(\dfrac{z_r}{z_0}\right)} \quad \text{and} \tag{A8}$$

$$U_s = U_r\frac{\ln\left(\dfrac{z_s}{z_0}\right)}{\ln\left(\dfrac{z_r}{z_0}\right)}. \tag{A9}$$

The standard deviation of the longitudinal velocity component ($\sigma_{u,s}$) is calculated from the product of Eq. (A6) and a reduction factor that accounts for short-duration block averaging and the mechanical response characteristics of the anemometer:

$$\sigma_{u,s} = \sigma_{u,\mathrm{Eq.(A6)}}\sqrt{\int_0^{\infty} S(n, z, z_0)\chi^2(\eta)\, df} \quad \text{and} \tag{A10}$$

$$\chi^2(\eta) = \left[\frac{\sin(\pi\eta t)}{\pi\eta t}\right]^2 \times \frac{1}{N^2}\left[\frac{\sin(\pi\eta\Delta N)}{\pi\eta\Delta}\right]^2 \times \frac{1}{1 + \left(\dfrac{2\pi\eta\lambda}{U_s}\right)^2}, \tag{A11}$$

where λ is the distance constant of the anemometer.

The bounding probabilities p (e.g., quartiles) are calculated from the Rice (1954) cumulative distribution function:

$$p = e^{-\upsilon T(\tilde{u}^2/2)} \quad \text{and} \tag{A12}$$

$$\upsilon^2 = \frac{\int_0^{\infty} f^2 S(n, z, z_0)\chi^2(\eta)\, df}{S(n, z, z_0)\chi^2(\eta)\, df}, \tag{A13}$$

where $\tilde{u}$ is the standardized gust speed calculated from the gust velocity U_s and the standard deviation of the surface wind speed σ_s, as determined from Eqs. (A5) and (A6):

$$\tilde{u} = U_S + u_s \sigma_s . \quad \text{(A14)}$$

The term υ, from Eq. (A13), is the nonzero up-crossing rate computed from the power spectral density filter function [Eq. (A4)] and $\chi^2(\eta)$ is the moving-average filter:

$$\chi^2(\eta) = \left[\frac{\sin(\pi\eta t)}{\pi\eta t}\right]^2 - \left[\frac{\sin(\pi\eta T)}{\pi\eta T}\right]^2, \quad \text{(A15)}$$

where t is the duration of the moving average used to compute the gust and T is the duration of the record containing the peak gust. The first filter term accounts for the short-duration averaging of the data. The second term accounts for the low-frequency energy that is not captured when the record duration is shorter than 30–60 min.

The abscissa was computed from

$$p = e^{-\upsilon T(u^2/2)} . \quad \text{(A16)}$$

REFERENCES

ASCE, 2010: Wind loads. *Minimum Design Loads for Buildings and Other Structures,* ASCE Standard Series, Vol. 7-10, ASCE, 241–258.

Balderrama, J. A., and Coauthors, 2011: The Florida Coastal Monitoring Program (FCMP): A review. *J. Wind Eng. Ind. Aerodyn.,* **99,** 979–995.

Barnes, S. L., 1964: A technique for maximizing details in numerical weather map analysis. *J. Appl. Meteor.,* **3,** 396–409.

Beljaars, A. C. M., 1987: The influence of sampling and filtering on measured wind gusts. *J. Atmos. Oceanic Technol.,* **4,** 613–626.

Beven, J. L., and Coauthors, 2008: Atlantic hurricane season of 2005. *Mon. Wea. Rev.,* **136,** 1109–1173.

Carbone, R. E., M. J. Carpenter, and C. D. Burghart, 1985: Doppler radar sampling limitations in convective storms. *J. Atmos. Oceanic Technol.,* **2,** 357–361.

ESDU, 1983: Strong winds in the atmospheric boundary layer. Part 2: Discrete gust speeds. Engineering Sciences Data Unit, Item No. 83045, HIS ESDU, London, United Kingdom.

FEMA, 2006: HAZUS MH MR3 hurricane model technical manual. Mitigation Division, Federal Emergency Management Agency, Dept. of Homeland Security. [Available online at www.fema.gov/library/viewRecord.do?id=3034.]

Foster, R. C., 2005: Why rolls are prevalent in the hurricane boundary layer. *J. Atmos. Sci.,* **62,** 2647–2661.

Franklin, J. L., M. L. Black, and K. Valde, 2003: GPS dropwindsonde wind profiles in hurricanes and their operational implications. *Wea. Forecasting,* **18,** 32–44.

Giammanco, I. M., J. L. Schroeder, and M. D. Powell, 2013: GPS dropwindsonde and WSR-88D observations of tropical cyclone vertical wind profiles and their characteristics. *Wea. Forecasting,* **28,** 77–99.

Greenway, M. E., 1979: An analytical approach to wind velocity gust factors. *J. Ind. Aerodyn.,* **5,** 61–91.

Harris, R. I., and D. M. Deaves, 1981: The structure of strong winds. *Proc. Conf. on Wind Engineering in the Eighties,* London, United Kingdom, Construction Industry Research and Information Association, Paper 4. [Available from CIRIA, Classic House, 174–180 Old St., London EC1V 9BP, United Kingdom.]

Hirth, B. D., J. L. Schroeder, C. C. Weiss, D. A. Smith, and M. I. Biggerstaff, 2012: Research radar analyses of the internal boundary layer over Cape Canaveral, Florida, during the landfall of Hurricane Frances (2004). *Wea. Forecasting,* **27,** 1349–1372.

Kepert, J. D., 2006: Observed boundary layer wind structure and balance in the hurricane core. Part I: Hurricane Georges. *J. Atmos. Sci.,* **63,** 2169–2193.

Kosiba, K. A., J. Wurman, and P. Robinson, 2012: Fine-scale Dual-Doppler analysis of the boundary layer in Hurricane Frances (2004). *Proc. 30th Conf. on Hurricanes and Tropical Meteorology,* Jacksonville, FL, Amer. Meteor. Soc. [Available online at https://ams.confex.com/ams/30Hurricane/webprogram/Paper205990.html.]

Lorsolo, S., J. L. Schroeder, P. Dodge, and F. Marks, 2008: An observational study of hurricane boundary layer small-scale coherent structures. *Mon. Wea. Rev.,* **136,** 2871–2893.

Majcen, M., P. Markowski, Y. Richardson, D. Dowell, and J. Wurman, 2008: Multipass objective analyses of Doppler radar data. *J. Atmos. Oceanic Technol.,* **25,** 1845–1858.

Masters, F. J., H. W. Tieleman, and J. A. Balderrama, 2010: Surface wind measurements in three Gulf coast hurricanes of 2005. *J. Wind Eng. Ind. Aerodyn.,* **98,** 533–547.

Morrison, I., S. Businger, F. Marks, P. Dodge, and J. A. Businger, 2005: An observational case for the prevalence of roll vortices in the hurricane boundary layer. *J. Atmos. Sci.,* **62,** 2662–2673.

Powell, M. D., and S. H. Houston, 1996: Hurricane Andrew's landfall in south Florida. Part II: Surface wind fields and potential real-time applications. *Wea. Forecasting,* **11,** 329–349.

——, ——, and T. A. Reinhold, 1996: Hurricane Andrew's landfall in south Florida. Part I: Standardizing measurements for documentation of surface wind fields. *Wea. Forecasting,* **11,** 304–328.

——, P. J. Vickery, and T. A. Reinhold, 2003: Reduced drag coefficient for high wind speeds in tropical cyclones. *Nature,* **422,** 279–283.

Rice, S. O., 1954: The mathematical analysis of random noise. *Noise and Stochastic Processes,* N. Wax, Ed., Dover Publications, 133–294.

Schroeder, J. L., and D. A. Smith, 2003: Hurricane Bonnie wind flow characteristics. *J. Wind Eng. Ind. Aerodyn.,* **91,** 767–789.

Simiu, E., and R. Scanlan, 1996: *Wind Effects on Structures: Fundamentals and Applications to Design.* 3rd ed. John Wiley and Sons, 688 pp.

Smith, R. K., and M. T. Montgomery, 2013: On the existence of the logarithmic surface layer in the inner core of hurricanes. *Quart. J. Roy. Meteor. Soc.,* doi:10.1002/qj.2121, in press.

Vickery, P. J., and P. F. Skerlj, 2005: Gust factors revisited. *J. Struct. Eng.,* **131,** 825–832.

——, D. Wadhera, M. D. Powell, and Y. Chen, 2009: A hurricane boundary layer and wind field model for use in engineering applications. *J. Appl. Meteor. Climatol.,* **48,** 381–405.

Wieringa, J., 1993: Representative roughness parameters for homogeneous terrain. *Bound.-Layer Meteor.,* **63,** 323–363.

Wurman, J., 2001: The DOW mobile multiple Doppler network. Preprints, *30th Int. Conf. on Radar Meteorology,* Munich, Germany, Amer. Meteor. Soc., 95–97.

——, and J. Winslow, 1998: Intense sub-kilometer boundary layer rolls in Hurricane Fran. *Science,* **280,** 555–557.

——, J. M. Straka, E. N. Rasmussen, M. Randall, and A. Zahrai, 1997: Design and deployment of a portable, pencil-beam, pulsed, 3-cm Doppler radar. *J. Atmos. Oceanic Technol.,* **14,** 1502–1512.